CHAPTER V

RESULTS AND DISCUSSION

This chapter can be divided into three main sections; i.e. 1) performance of fixed-bed reactor and membrane reactor, 2) comparison between different mathematical models and 3) membrane reactor study. The mathematical models were developed to simulate the dehydrogenation of ethylbenzene to styrene in fixed-bed reactors and membrane reactors. The kinetic data of the commercial catalyst consisting of Fe_2O_3 and K_2O oxides and permeation data of hydrogen through a palladium membrane were taken from Abdalla *at al. (1994)* and Hermann *et al. (1997)*, respectively. Tables 5.1 to 5.4 provided the standard operating conditions and simulation parameters of the fixed-bed reactor and the membrane reactor. The simplified reaction scheme of the ethylbenzene dehydrogenation is illustrated in Figure 5.1. The major side products are benzene, toluene, methane, ethylene and carbon oxides.

Table 5.1 Simulation parameters[Hermann *et al.*, 1997 and Abdalla *et al.*, 1994)

Parameters	Unit	Value
Inner radius of inner tube	[m]	5×10^{-3}
Outer radius of inner tube	[m]	7×10^{-3}
Inner radius of outer tube	[m]	8.61×10^{-3}
Outer radius of outer tube	[m]	10.61×10^{-3}
Total membrane length (l_0)	[m]	150×10^{-3}
Cross section area of reaction side	[m]	7.86×10^{-5}
Catalyst properties (Fe_2O_3 and K_2CO_3)		
- Density	[kg/m^3]	1500
- Porosity	[-]	0.5

Table 5.2 Standard operating condition (form optimum condition in the fixed-bed reactor)

Operating conditions	Unit	Value
Operating temperature	[K]	923
Total pressure in reaction side	[Pa]	1.2×10^{5}
Total pressure in separation side	[Pa]	1.2×10^{5}
W_{cat}/F_{EB0}	[kg_{cat} s/mol]	1027.2
S/O (Ethylbenzene/Steam)	[-]	6
Feed flow rate of ethylbenzene	[mol/s]	1.72×10^{-5}
Inert sweep gas flow rate	[mol/s]	8.6×10^{-4}
Reactive sweep gas flow rate	[mol/s]	8.6×10^{-4}

Table 5.3 Membrane properties [Hermann, *et al.* 1997]

Parameter	Unit	Value
Separative Pd layer	[m]	10×10^{-6}
Outer diameter of support tube	[m]	14×10^{-3}
Inner diameter of support tube	[m]	10×10^{-3}
Permeation coefficient of hydrogen through the membrane	$[mol/m\cdot s\cdot Pa^{0.5}]$	$2.03\times10^{-7}\cdot e^{(-21700\ RT)}$ $\times3.03\times10^{5}\cdot T^{-1.0358}$

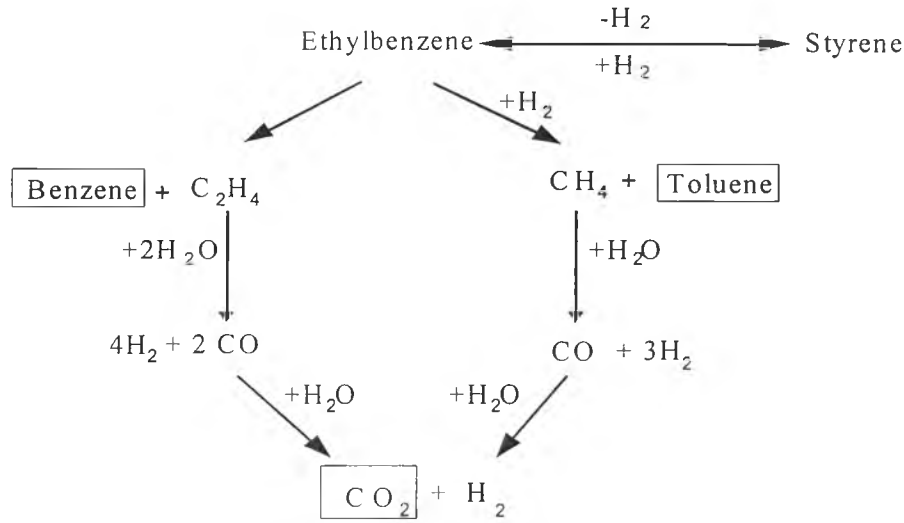

Figure 5.1 Simplified reaction scheme of ethylbenzene dehydrogenation

Table 5.4 Catalytic reaction model of catalytic dehydrogenation of ethylbenzene [Abdalla *et al.*1994]

Reaction number	Reaction	Rate equation	A_i^*	E_i^{**}
1	$EB \leftrightarrow S + H_2$	$r_1 = k_1\left(P_{EB} - \frac{P_S P_H}{K_{EB}}\right)$	0.851	90891
2	$EB \rightarrow B + C_2H_4$	$r_2 = k_2 P_{EB}$	14.00	207989
3	$EB + H_2 \rightarrow T + CH_4$	$r_3 = k_3 P_{EB} P_H$	0.56	9151
4	$H_2O + \frac{1}{2}C_2H_4 \rightarrow CO + 2H_2$	$r_4 = k_4 P_{HO} P_{C_2H_4}^{0.5}$	0.12	103996
5	$H_2O + CH_4 \rightarrow CO + 3H_2$	$r_5 = k_5 P_{HO} P_{CH_4}$	-3.21	65723
6	$H_2O + CO \rightarrow CO_2 + H_2$	$r_6 = k_6 P_{HO} P_{CO}$	21.24	73628

* A_{1i} Pre-exponential factor(dimensionless) [$k_i = \exp(A_i - E_i / RT)$].

** E_{ii} Activation energy of reaction is (kJ/mol).

*** $K_{EB} = \exp(\Delta F_0 / RT)$, $\Delta F_0 = a + bT + cT^2$, a = 122725.157 kJ/kmol , b = -12627 kJ/mol K , $c = -2.194 \times 10^{-3}$ kJ/kmol K^2

k_i = reaction i rate constant (mol/g sec Pa^n), n = 1 for k_1 and k_2, n = 2 for k_3 and k_5, n = 1.5 for k_4 and k_6 mol K^3/g sec Pa^3

5.1 Performance of fixed-bed and membrane reactor

In this part, the isothermal and plug flow conditions were assumed for both the fixed-bed and the membrane reactor. It is aimed to understand the catalytic behavior of the reactors at various operating conditions.

5.1.1 Performance of fixed-bed reactor

Effect of W_{cat}/F_{EB0}

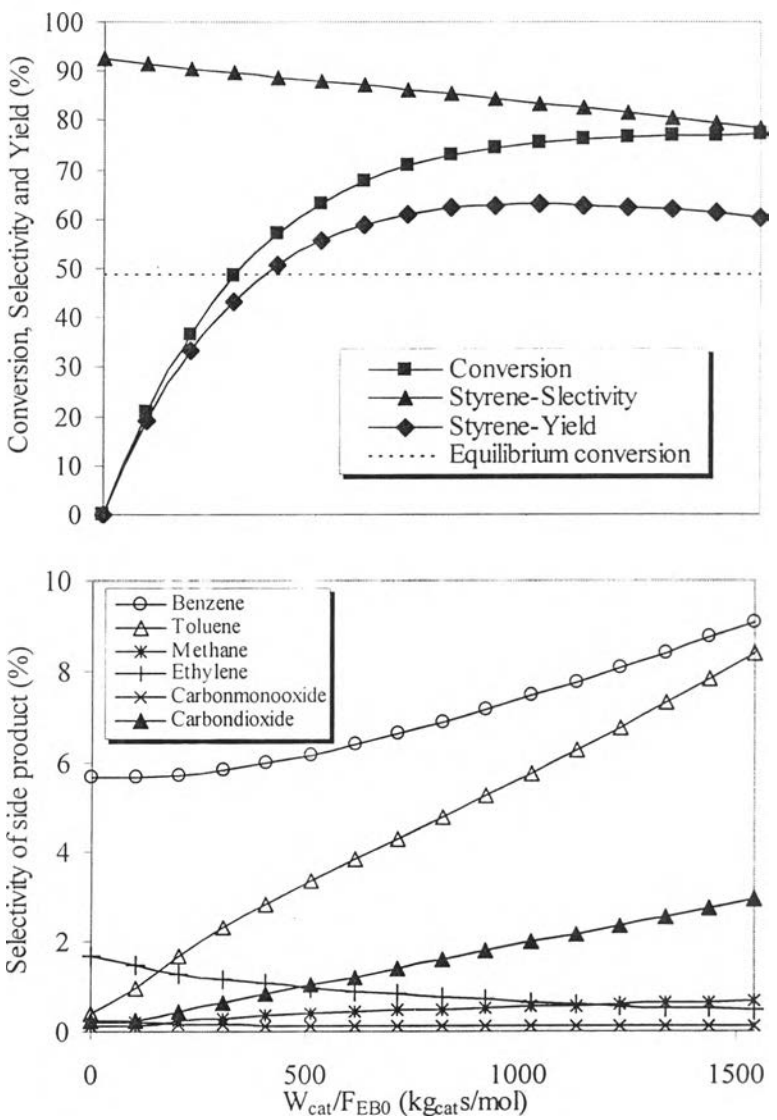

Figure 5.2 Effect of W_{cat}/F_{EB0} on performance of fixed-bed reactor (T = 900 K, S/O = 6, P= 1.2×10^5 Pa)

Figure 5.2 shows the performance of the fixed-bed reactor as a function of catalyst weight to molar feed rate of ethylbenzene (W_{cat}/F_{EB}). It was found that increasing W_{cat}/F_{EB} increased the ethylbenzene conversion but decreased the selectivity to the desired product, styrene. The selectivities to benzene, toluene and carbon dioxide increased with increasing W_{cat}/F_{EB} because they were final products of the system. The selectivity to ethylene showed different trend due to the subsequent conversion to carbon monoxide. The optimum W_{cat}/F_{EB} was found to be 1027.2 kg_{cat}·s/mol. It should be noted that due to the presence of side reactions the obtained conversion was higher than the equilibrium value.

Effect of steam/ethylbenzene ratio (S/O)

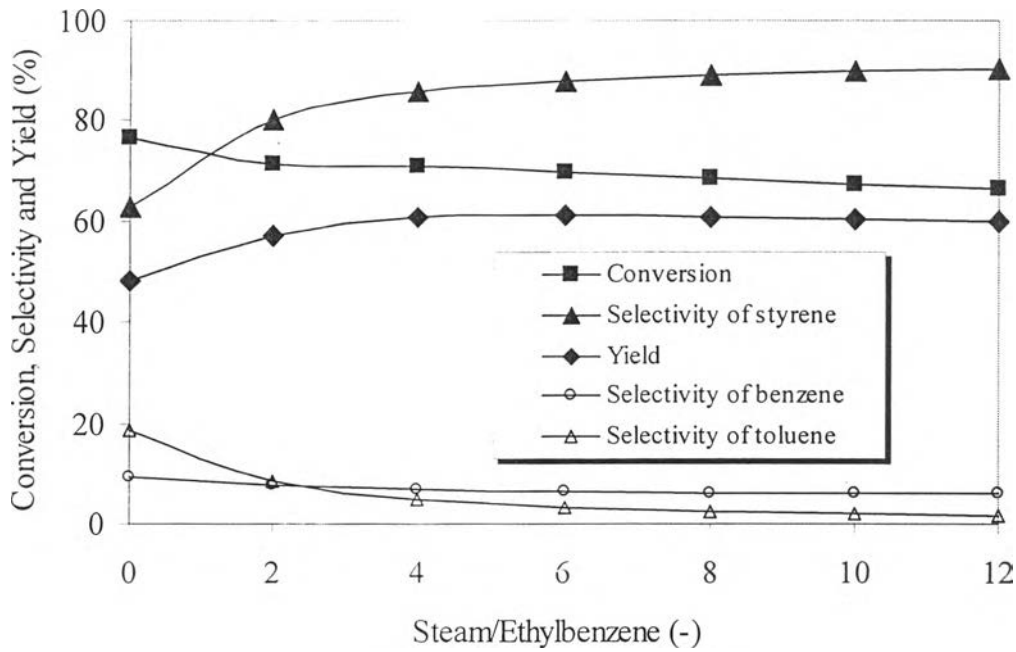

Figure 5.3 Effect of steam/ethylbenzene ratio on performance of fixed-bed reactor

($T = 900$ K, $P = 1.2 \times 10^5$ Pa, $W_{cat}/F_{EBO} = 1160$ kg_{cat} s/mol)

Steam is usually added to the feed in order to suppress the catalyst deactivation. A commercial operation uses steam/hydrocarbon (S/O ratio) ranging between 6-12 (Hermann *et al.*, 1997). Figure 5.3 shows the effect of S/O ratio on the performance of the fixed-bed reactor. Increasing the amount of steam in the feed

reduced the partial pressure of ethylbenzene, as a result, the reaction rate decreased. This was noticed by the decrease of conversion with increasing the S/O ratio. In addition, the similar result that the selectivity to styrene decreased with the increasing extent of reaction was also observed here. Consequently, there existed an optimum S/O which was around 6 in this system.

Effect of operating pressure

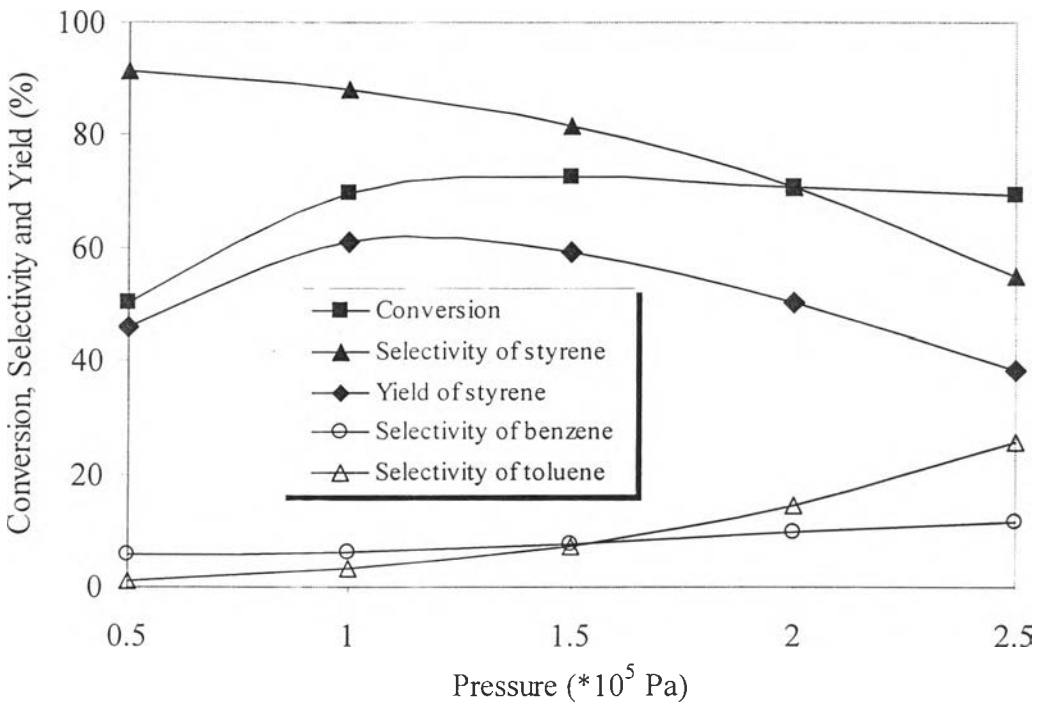

Figure 5.4 Effect of pressure on performance of fixed-bed reactor (T = 900 K, S/O = 6, W_{cat}/F_{EBO} = 1160 kg_{cat} s/mol)

It was found that increasing operating pressure increased the conversion of ethylbenzene; however, it reached the maximum value and then gradually decreased. This result can be explained by the presence of two opposing trends from the change of operating pressure. The higher pressure increased the partial pressure of the reactant and, hence, the rate of reaction became higher. However, it shifted the equilibrium conversion backwards. It is noted that became the main reaction involved the increased number of moles in the reaction system, the increased pressure of the

system tended to shift the reaction backward according to the Le Chatelier's principle (Atkins,1994). It was also found that the selectivity to styrene decreased with the increasing pressure and that the optimum pressure of 1.2×10^5 Pa was observed.

Effect of temperature

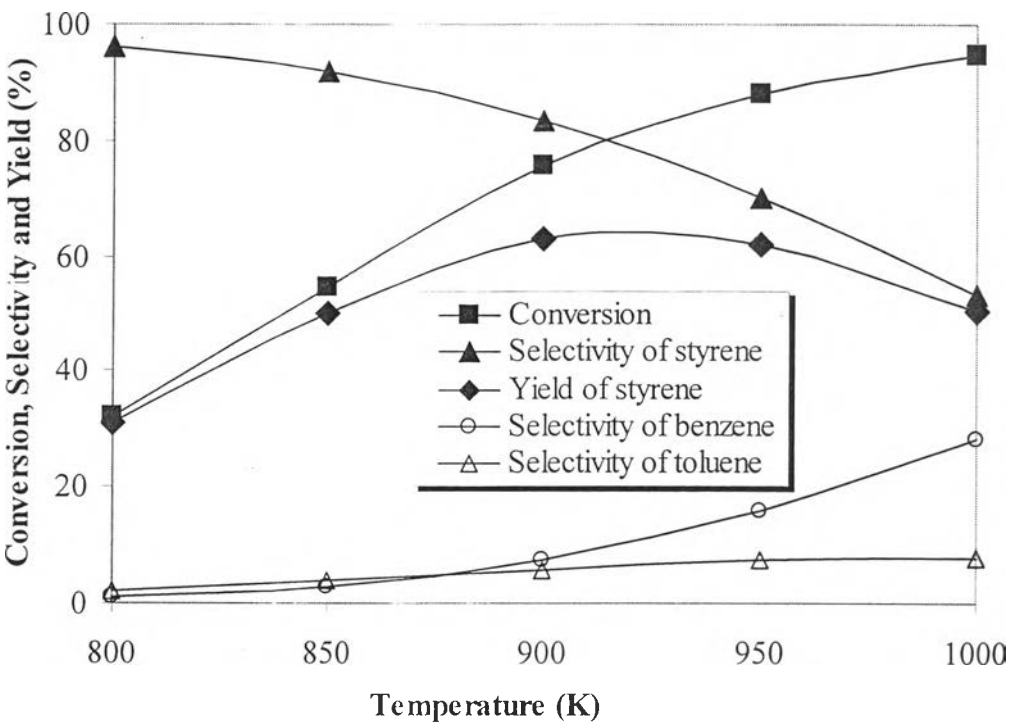

Figure 5.5 Effect of Temperature on performance of fixed-bed reactor ($P=1.2 \times 10^5$ Pa, S/O = 6, W_{cat}/F_{EBO} = 1027.2 kg_{cat} s/mol)

Figure 5.5 shows the performance of the fixed-bed reactor at various operating temperatures. The conversion of ethylbenzene, selectivity of styrene, selectivity of benzene and toluene and yield of styrene were presented. Since the equilibrium conversion is function of temperature, the increase of the reaction temperature increased the conversion of ethylbenzene at the price of lower selectivity to styrene due to the presence of side reactions. The optimum yield was observed at the operating temperature of 923 K.

In the subsequent parts, the operating condition was based on the condition of T = 923 K, P = 1.2×10^5 Pa, S/O = 6 and W_{cat}/F_{EB0} = 1027.2 kg_{cat} s/mol .

5.1.2 Performance of membrane reactor

This section aims to illustrate the performance of a membrane reactor compared with that of the fixed-bed reactor. The membrane reactor is a double tubular configuration with a catalyst bed packed in the tube of palladium membrane. Inert sweep gas of nitrogen was fed to the annular (or shell side) to remove permeating hydrogen from the reactor. The basic assumptions of isothermal, isobaric, and plug flow condition within both reactors were used in the simulations. Figures 5.6 and 5.7 show the performance of reactor while Figure 5.8 shows the partial pressure of components in the reactor.

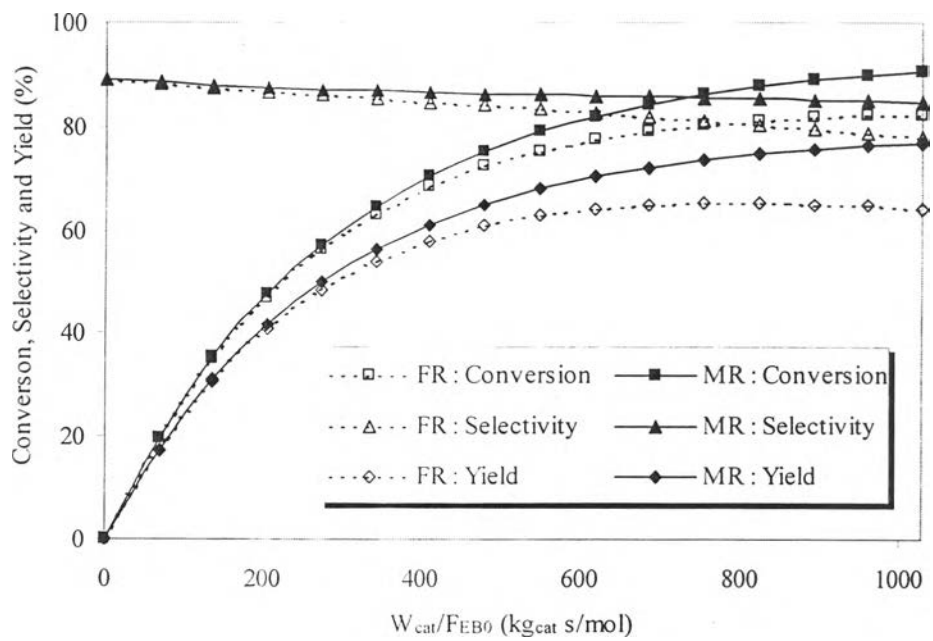

Figure 5.6 Performance of fixed-bed reactor and membrane reactor from ideal model (T = 923 K, $P_{reaction\ side} = 1.2 \times 10^5$ Pa, $P_{separation\ side} = 1.2 \times 10^5$ Pa, S/O = 6 W_{cat}/F_{EB0} = 1027.2 kg_{cat} s/mol)

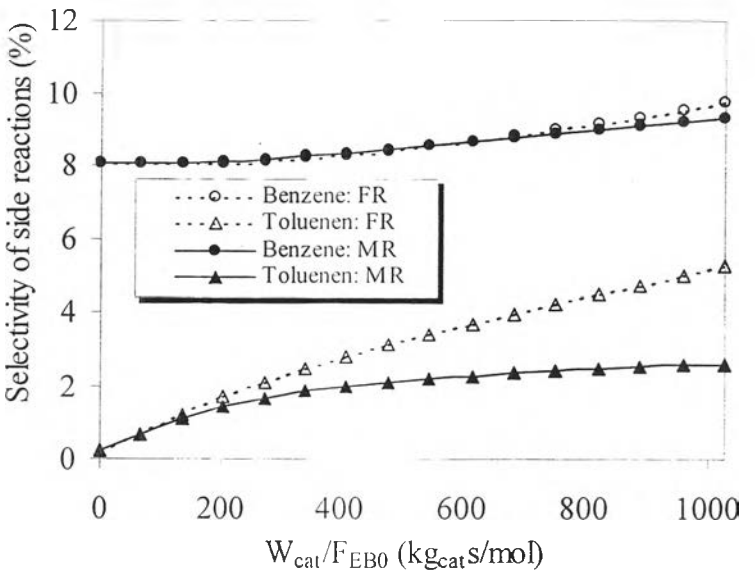

Figure 5.7 Selectivity of side reactions in fixed-bed reactor and membrane reactor from ideal model (T = 923 K, $P_{\text{reaction side}} = 1.2\times10^{5}$ Pa, $P_{\text{separation side}} = 1.2\times10^{5}$ Pa, S/O = 6, $W_{cat}/F_{EB0} = 1027.2$ kg_{cat} s/mol)

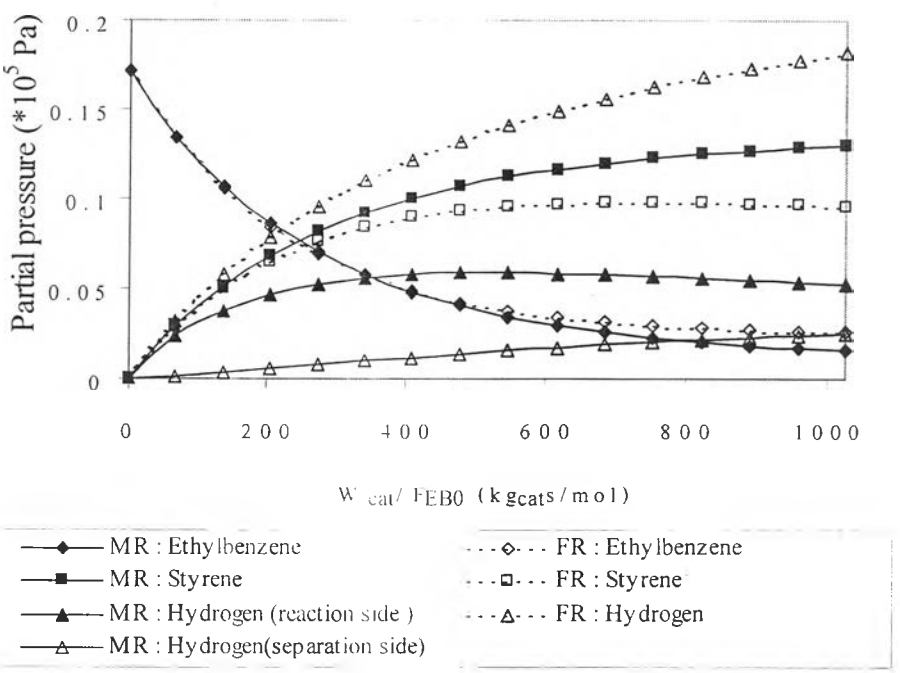

Figure 5.8 Partial pressure profile of reaction mixture in fixed-bed reactor and membrane reactor (T = 923 K, $P_{\text{reaction side}} = 1.2\times10^{5}$ Pa, $P_{\text{separation side}} = 1.2\times10^{5}$ Pa, S/O = 6 $W_{cat}/F_{EB0} = 1027.2$ kg_{cat} s/mol)

From Figure 5.6 it was found that the membrane reactor (MR) was superior to the fixed-bed reactor (FR) in both conversion and selectivity. The yield of membrane reactor becomes higher with the increasing W_{cat}/F_{EB}. Figure 5.7 shows that the formation of toluene (reaction No.3 from Table 5.4) was suppressed with the use of the membrane reactor because hydrogen was removed from the reaction zone through the membrane as found in Figure 5.8 that the partial pressure of hydrogen in the reaction zone in the membrane reactor was much lower than that in the fixed-bed reactor. This also enhanced the forward reaction to the desired product, styrene, and resulted in higher reaction conversion. It can be concluded that the membrane reactor can help improve the performance of the conventional reactor on both shifting the extent of reaction and the selectivity to the desired product.

5.2 Comparison between different mathematical models

In the past, most of investigators employed simple mathematical model assuming isothermal and plug-flow condition to simulate behaviors of many dehydrogenation reactions in membrane reactors. In this section, the comparisons between the results of the three models; i.e. 1) isothermal and plug flow model (IP), 2) non isothermal and plug flow model (NIP) and 3) non isothermal with radial dispersion model (NIR), were illustrated for both fixed-bed reactor and membrane reactor. Due to the high endothermicity of this reaction, the isothermal model may not describe the behaviors of the reaction system accurately. In addition, the presence of the radial heat and mass dispersion may cause assumption of the plug flow condiation unrealistic.

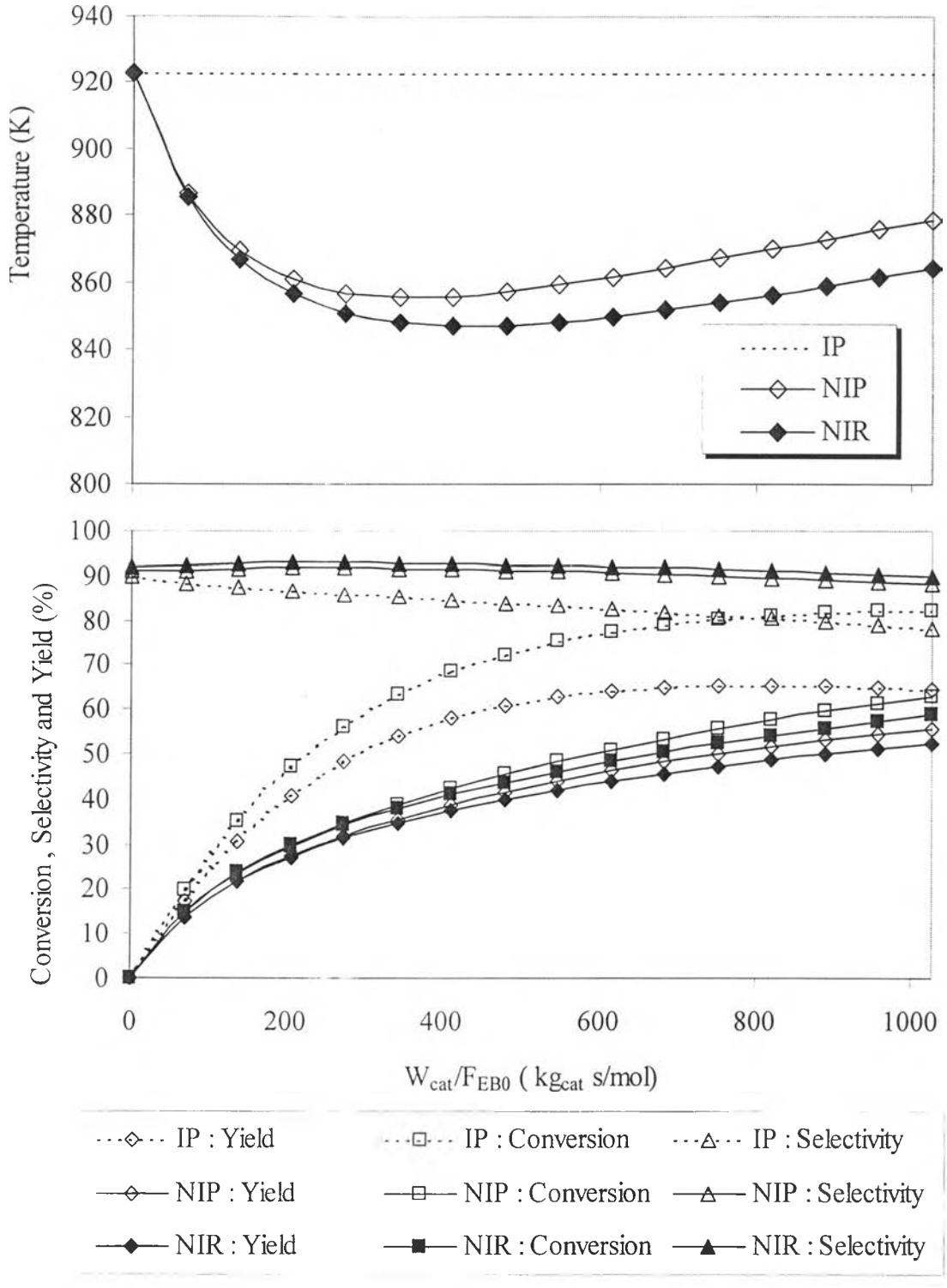

Figure 5.9 Effect of heat and radial dispersion on the fixed-bed reactor ($F_{EB0} = 1.72 \times 10^{-5}$ mol/s, $T_{reaction\ side} = 923$ K, $T_{ss} = 923$ K, $P = 1.2 \times 10^{5}$ Pa, S/O = 6)

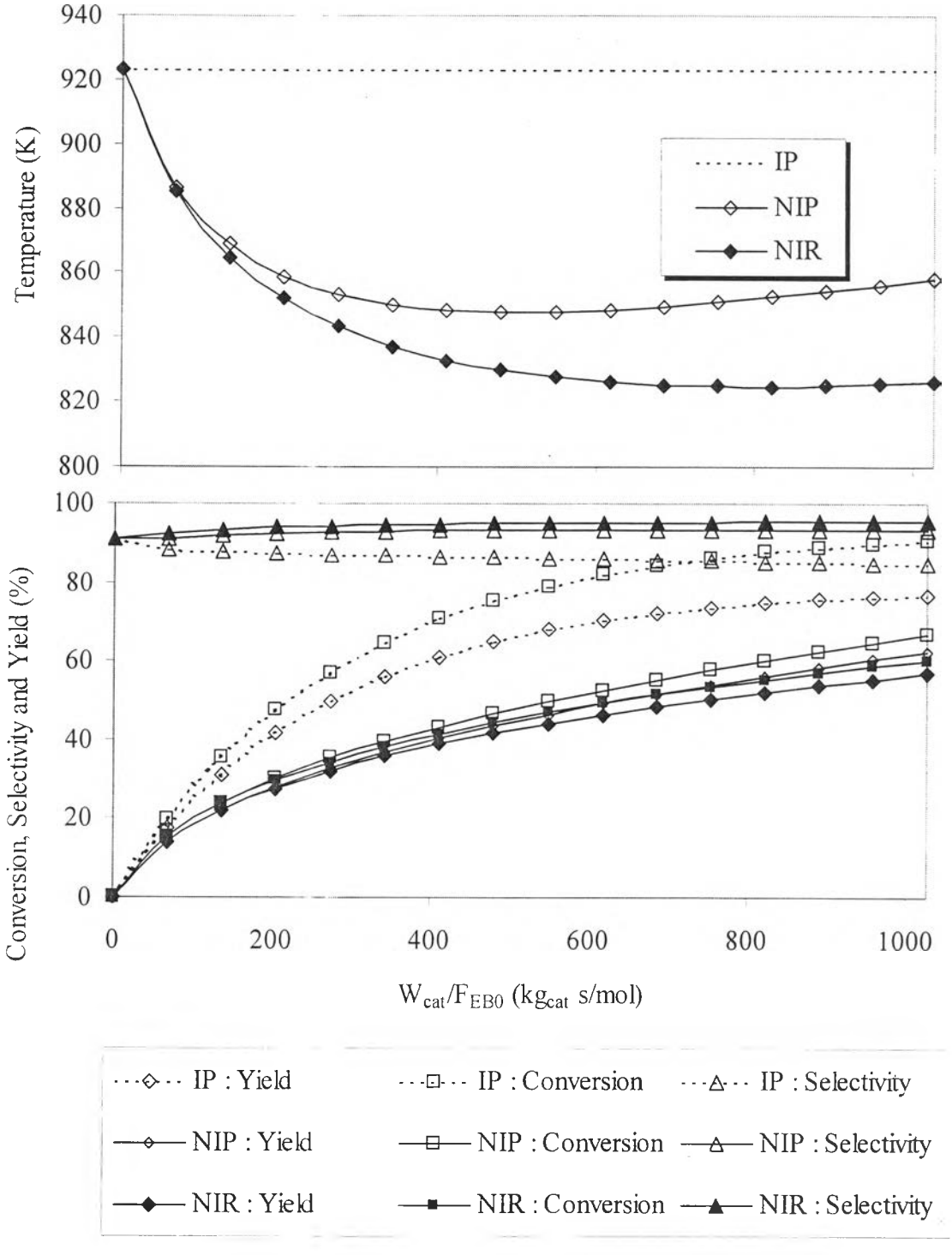

Figure 5.10 Effect of heat and radial dispersion on the membrane reactor (F_{EB0} $=1.72\times10^{-5}$ mol/s, Inert sweep flow $= 8.60\times10^{-5}$ mol/s, $T_{reaction\ side}$ = 923 K, $T_{separation\ side}$ = 900 K, T_{ss} = 923 K, $P_{reaction\ side}$ = 1.2×10^{5} Pa, $P_{sep} = 1.2\times10^{5}$ Pa, S/O = 6 W_{cat}/F_{EB0} = 1027.2 kg_{cat} s/mol)

Figure 5.9 compares the simulation results of the temperature profiles and the reactor performance from three different models of the fixed bed reactor. It was assumed that the wall temperature was constant along the reactor length. Due to the high endothermicity of this reaction, the isothermal model may not describe the behaviors of the reaction system accurately. It was clearly found that the assumption of isothermal condition or even the omission of certain thermal phenomena that took place inside the reactor, led to a significant overestimation of the temperature profile along the bed length. The temperature dropped at the beginning of the bed due to high extent of reaction, which resulted in the high heat consumption. The temperature started increasing again because the rate of heat transfer to the catalyst bed is higher than the rate of heat of reaction. As a result, there is a cold spot temperature, which is a common problem for an endothermic reaction system, in the reactor. In addition, the results revealed that the plug flow condition was not an appropriate assumption because the slow rate of radial dispersion retarded the heat transfer from the reactor wall to the catalyst bed. Considering the conversion of the reactor, it was clearly seen that neglecting the heat effect can cause significant error. This result was also observed for the radial dispersion effect but the deviation was much smaller. The values of the selectivity from the isothermal and plug flow model were found lower than those from the other models. This can be explained by result found in the earlier section that the selectivity decreased with the increasing operating temperature. The resulting yield corresponded to the respective conversion and selectivity.

Figure 5.10 compares the results for the membrane reactor. It was found that the results followed the same trends as found in the fixed-bed reactor. As a result, it can be concluded that the assumptions of isothermal and plug flow condition are not suitable for this system. Consequently, the subsequent investigations on the performance of the membrane reactor will be carried out based on the model taking into account of both non-isothermal and radial dispersion effects.

5.3 Membrane reactor study

5.3.1 Comparison between catalyst bed packed in the tube side and the shell side

The membrane reactor is a double tube configuration with a conventional fixed-bed of catalyst surrounded by the membrane. The location of catalyst may be either in the tube side or in the shell side.

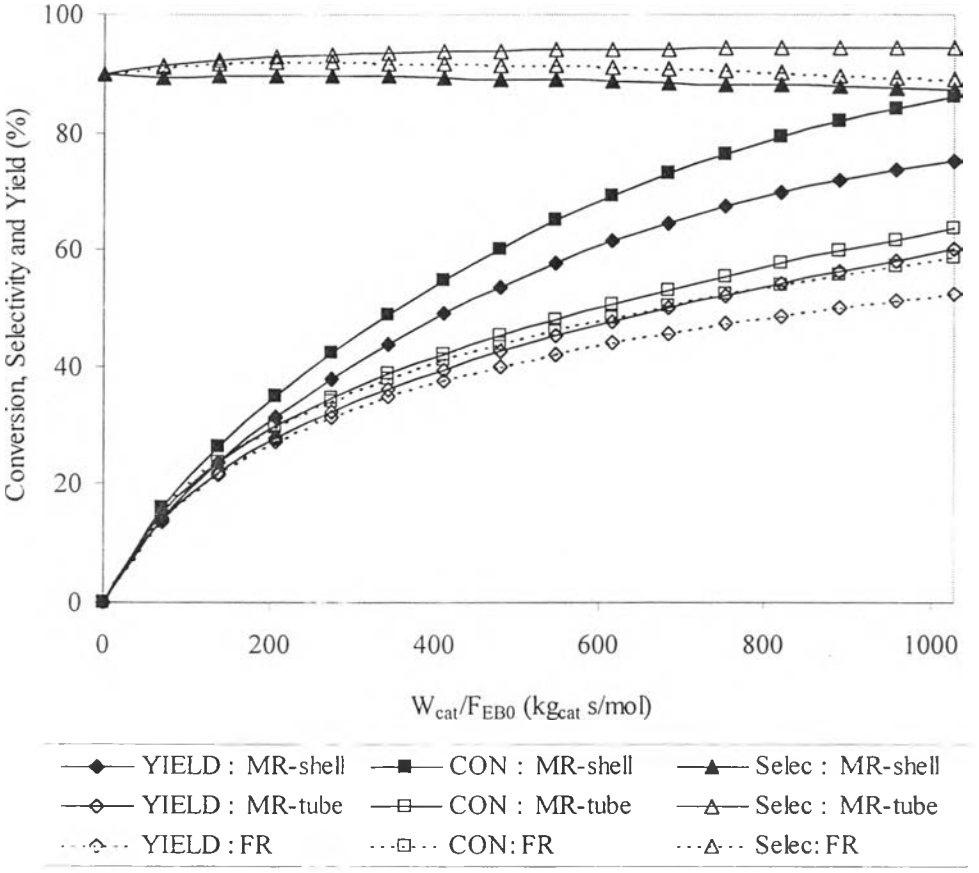

Figure 5.11 Comparison between packing catalyst bed in tube side or shell side ($F_{EB0} = 1.72 \times 10^{-5}$ mol/s, Inert sweep flow $= 8.60 \times 10^{-5}$ mol/s, $T_{\text{reaction side}} = 923$ K, $T_{\text{separation side}} = 900$ K, $T_{ss} = 923$ K, $P_{\text{reaction side}} = 1.2 \times 10^{5}$ Pa, $P_{\text{separation side}} = 1.2 \times 10^{5}$ Pa, S/O = 6)

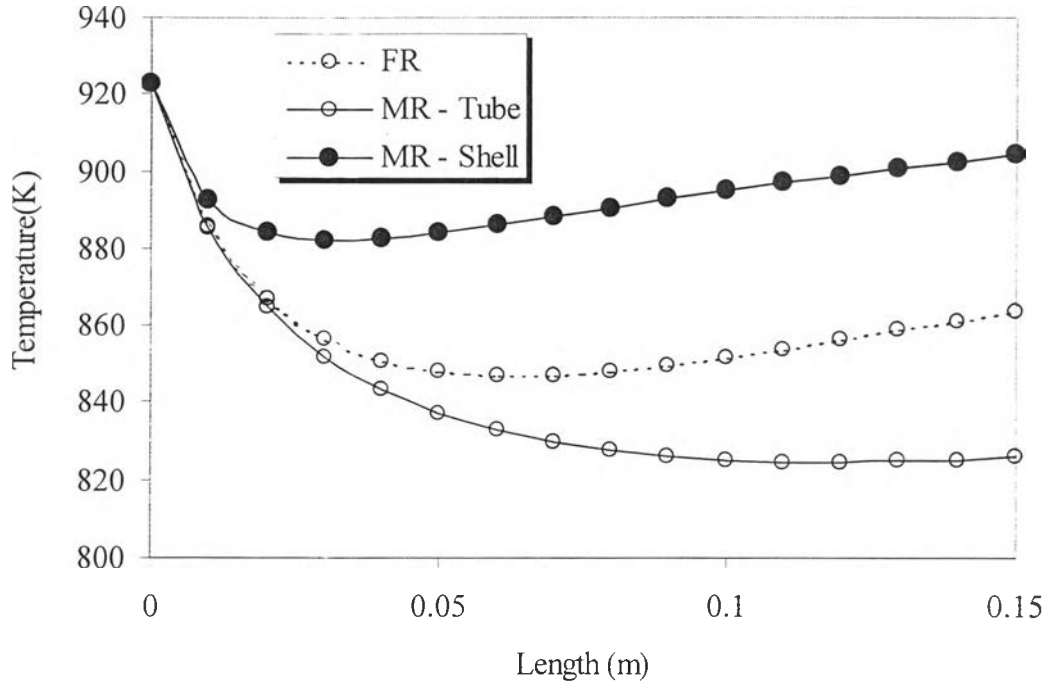

Figure 5.12 Temperature profile along the reactor length ($F_{EB0} = 1.72 \times 10^{-5}$ mol/s, Inert sweep flow $= 8.60 \times 10^{-5}$ mol/s, $T_{\text{reaction side}} = 923$ K, $T_{\text{separation side}} = 900$ K, $T_{ss} = 923$ K, $P_{\text{reaction side}} = 1.2 \times 10^{5}$ Pa. $P_{\text{separation side}} = 1.2 \times 10^{5}$ Pa, S/O = 6)

Figures 5.11 and 5.12 show the reactor performance and the temperature profiles of the membrane reactors compared with the conventional fixed-bed reactor, respectively. The membrane reactors were divided into two cases; i.e. the one with the catalyst packed in the tube side and the other with the catalyst packed in the shell side. The amount of catalyst for all case were the same. It was found that the membrane reactor with the catalyst bed in the shell side provided the best conversion and yield. This can be explained by considering the temperature profile along the reactors. Because the catalyst was packed in the shell side, heat can transfer directly to the catalyst bed like in the conventional fixed-bed reactor. However, with the larger heat transfer area in the membrane reactor, the temperature along the reactor length followed the sequence: membrane reactor with packed catalyst in the shell side > fixed-bed reactor > membrane reactor with catalyst packed in the tube. The temperature of the membrane reactor with catalyst packed in the tube was lower than

the fixed-bed reactor because the additional heat transfer resistance of the sweep gas. It should be emphasized the advantage of the membrane reactor that in spite of the lower temperature of the membrane reactor with the catalyst in the tube, the conversion and yield were superior to the fixed-bed reactor.

It can be concluded from the results that the membrane reactor with the catalyst packed in the shell side was superior to the one with the catalyst packed in the tube side due to the lower heat transfer resistance.

5.3.2 Effect of operating modes in the separation side

The membrane reactor concept applied to dehydrogenation reaction is based on the removal of product hydrogen from the reaction zone so that the obtained conversion can exceed the equilibrium value. There are a number of methods employed to promote the rate of hydrogen removal. The main concept is to increase the driving force, which is the difference in partial pressure of hydrogen between the reaction side and the separation side. This can be carried out under different modes such as using vacuum in the separation side, introducing inert sweep gas to reduce the partial pressure of hydrogen in the sweep side or performing coupling reaction so that the product hydrogen is simultaneously consumed by the other reaction in the opposite side of the catalyst bed.

Table 5.5 compares the performance of the membrane reactor under three different modes; namely vacuum, inert sweep gas at two flow rates of 1.72×10^{-4} and 8.60×10^{-4} mol/s and reactive sweep gas, which is air in this study. Oxygen reacts with hydrogen, forming water and heat. Figure 5.13 shows the ratio of the partial pressure difference of hydrogen between the reaction side and the separation side over the partial pressure of hydrogen in the reaction side and the temperature profiles of the catalyst bed under different modes of operation. The catalyst bed was packed in the shell side to obtain high heat transfer.

Table 5.5 Effect of sweep mode ($F_{EB0} = 1.72 \times 10^{-5}$ mol/s, T = 900 K, T_{sep} = 900K, T_{ss} = 923 K, P_r=1.2×10^5 Pa , inert sweep flow rate =$1.72 \times 10^{-4} - 1.72 \times 10^{-3}$ mol/s, reactive sweep flow rate = 8.60×10^{-4} mol/s, S/O = 6, W_{cat}/F_{EB0} = 1027.2 $kg_{cat}s/mol$ and membrane reactor with thickness of 10μm)

Mode of separation side	Ethylbenzene Conversion (%)	Styrene Selectivity(%)	Styrene Yield(%)
Inert sweep gas various flow rate (mol/s)			
• 1.72×10^{-4}	81.3	86.7	70.5
• 8.60×10^{-4}	86.0	87.4	75.2
Vacuum	89.2	88.0	78.5
Reactive sweep gas	93.7	78.3	73.4

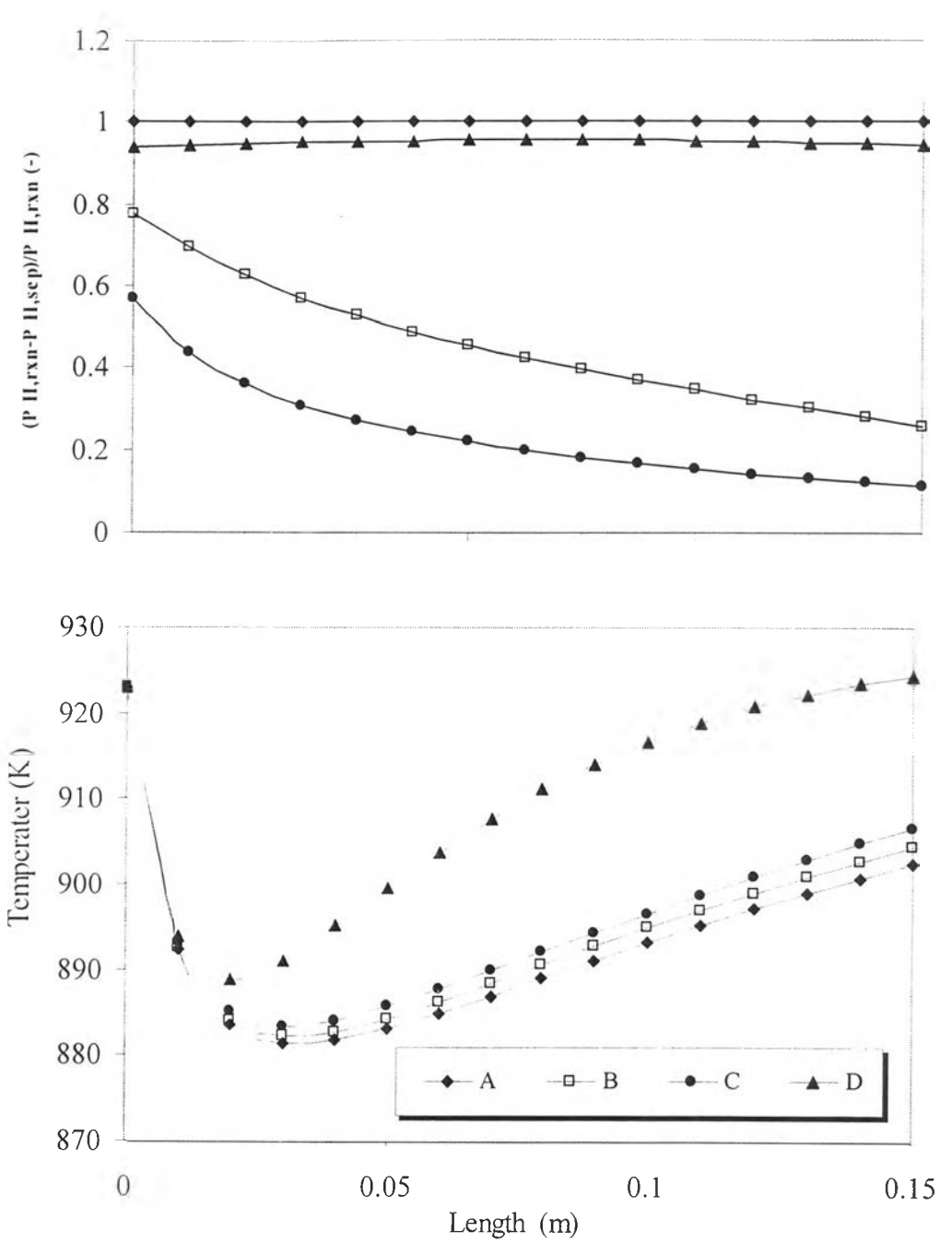

Figure 5.13 Partial pressure and temperature profile along the reactor length at various operating modes in separation side, i.e.,

A) vacuum application

B) inert sweep flow as nitrogen at 8.60×10^{-4} mol/s

C) inert sweep flow as nitrogen at 1.72×10^{-4} mol/s

D) reactive sweep flow as air at 8.60×10^{-4} mol/s

($F_{EB0} = 1.72 \times 10^{-5}$ mol/s, $T_{reaction\ side} = 900$ K, $T_{separation\ side} = 900$K, $T_{ss} = 923$ K, $P_{reaction\ side} = 1.2 \times 10^{5}$ Pa, $P_{sepration\ side} = 1.2 \times 10^{5}$ Pa, S/O = 6, $W_{cat}/F_{EB0} = 1027.2\ kg_{cat}s/mol$)

It was found by considering the ratio of the partial pressure difference of hydrogen between the reaction side and the separation side over the partial pressure of hydrogen in the reaction side that the reaction between oxygen and hydrogen was almost complete along the reactor length. The ratio was close to 1, which was the case of the vacuum mode in which all permeating hydrogen was entirely removed from the separation zone. Hydrogen partial pressure was gradually accumulated along the reactor length in the inert sweep gas mode as found that the ratio decreased with the increasing reactor length. The increasing inert sweep flow rate also increased the driving force of partial pressure difference of hydrogen. Considering the temperature profile shows that the exothermic heat from the combustion of hydrogen supplied additional heat to the catalyst bed, and, as a result, the temperature of the bed for the reactive sweep gas case was the highest compared to the other case. The temperature of the reaction zone decreased with the increasing amount of hydrogen removal; i.e. inert sweep gas of 1.72×10^{-4} mol/s > inert sweep gas of 8.60×10^{-4} mol/s > vacuum mode. However, the differences were not pronounced.

Table 5.5 shows that increasing the hydrogen removal by increasing the inert sweep flow rate resulted in higher reaction conversion and selectivity (by suppressing the side reaction between hydrogen and the reactant) and, thus, increased in yield. The value at high sweep flow rate become close to the vacuum mode case which represented the maximum driving force of the partial pressure difference of hydrogen. It should be noted that for the reactive sweep gas case, even though the conversion became much higher but the selectivity, on the other hand, dropped with the resulting higher temperature. It was found that the obtained yield became even smaller than the case with the inert sweep gas with the flow rate of inert sweep gas of 8.60×10^{-4} mol/s and the vacuum in the separation side.

5.3.3 Influence of diameter of the reaction side

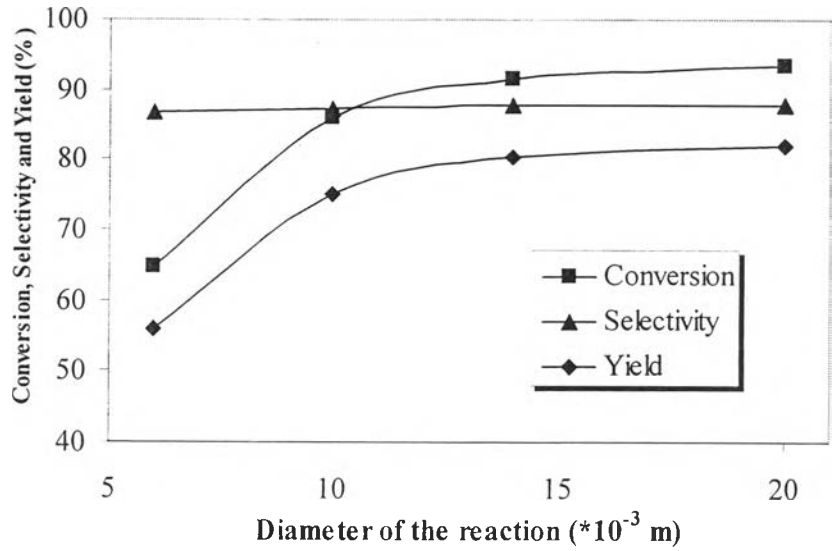

Figure 5.14 Influence of Diameter of the reaction ($F_{EB0} = 1.72 \times 10^{-5}$ mol/s, Inert sweep flow = 8.60×10^{-5} mol/s, $T_{reaction\ side}$ = 923 K, $T_{separation\ side}$ = 923K, T_{ss} = 923 K, $P_{reaction\ side} = 1.2 \times 10^{5}$ Pa , $P_{separation\ side} = 1.2 \times 10^{5}$ Pa , S/O = 6 and catalyst was packed in the shell side)

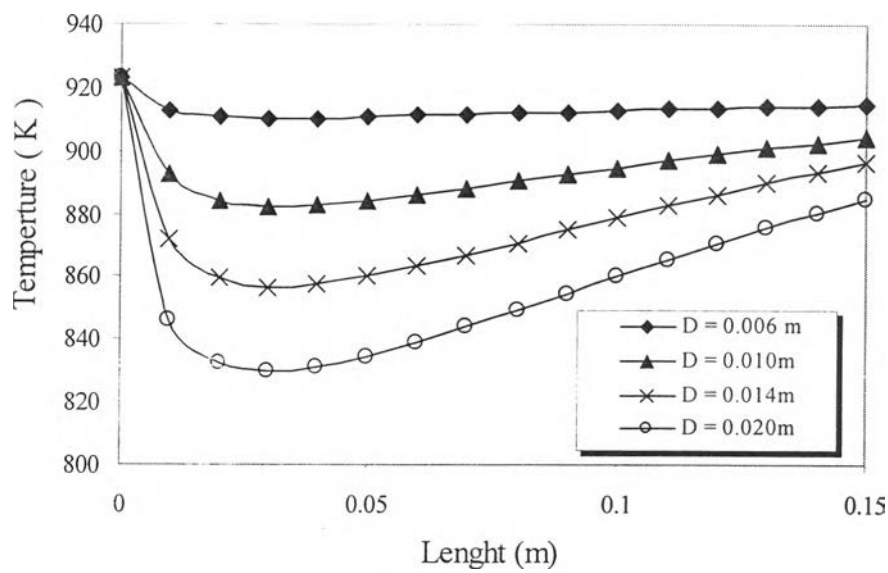

Figure 5.15 Temperature profile along the reactor length with various diameter of the reaction($F_{EB0} = 1.72 \times 10^{-5}$ mol/s, Inert sweep flow = 8.60×10^{-5} mol/s, $T_{reaction\ side}$ = 923 K, $T_{separation\ side}$ = 923K, T_{ss} = 923 K, $P_{reaction\ side} = 1.2 \times 10^{5}$ Pa , $P_{separation\ side} = 1.2 \times 10^{5}$ Pa , S/O = 6 and catalyst was packed in the shell side)

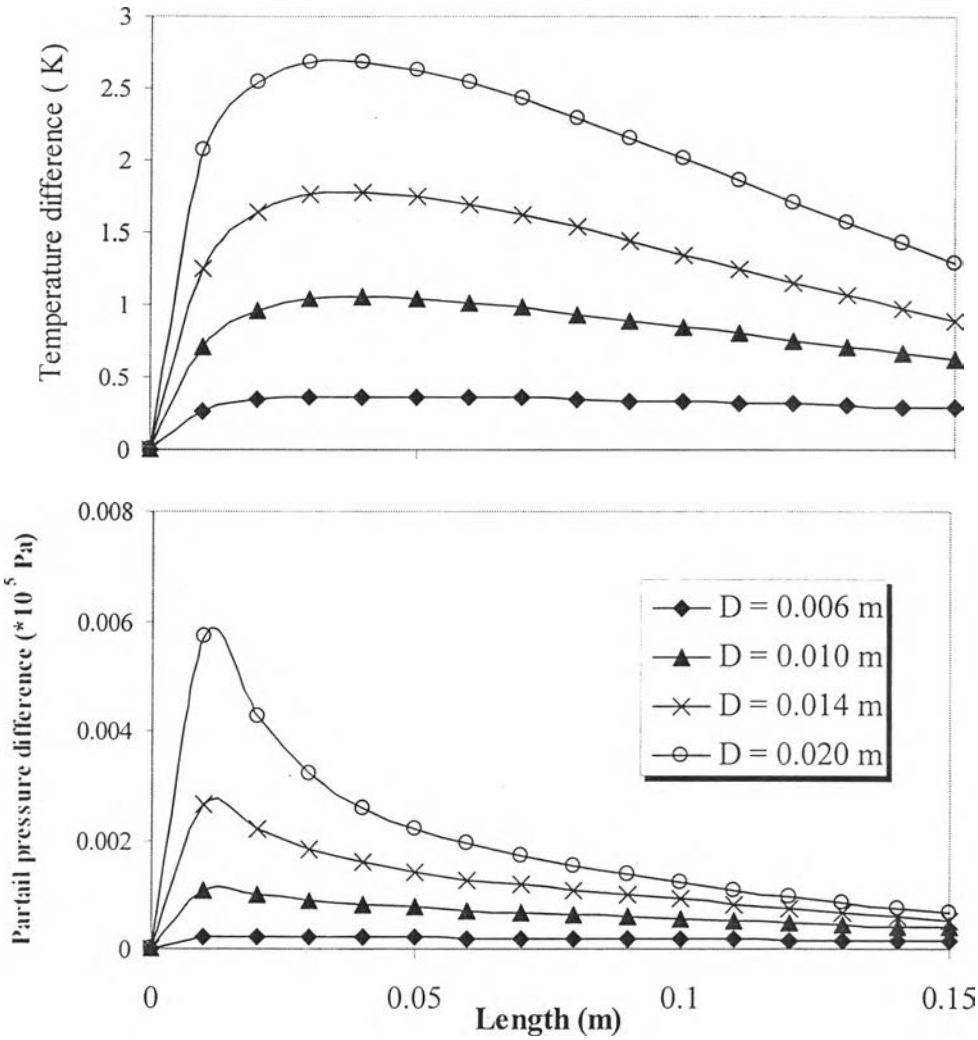

Figure 5.16 Profiles of differences of temperature and partial pressure of hydrogen between the reactor wall and the membrane surface ($F_{EB0} = 1.72 \times 10^{-5}$ mol/s, Inert sweep flow = 8.60×10^{-5} mol/s, $T_{reaction\ side} = 923$ K, $T_{separation\ side} = 923$K , $T_{ss} = 923$ K, $P_{reaction\ side} = 1.2 \times 10^{5}$Pa , $P_{separaation\ side} = 1.2 \times 10^{5}$Pa , S/O = 6, catalyst was packed in shell side)

Figure 5.14 shows the effect of the reactor diameter on the performance of the membrane reactor operated under the inert sweep flow mode. It should be noted that increasing the reactor diameter did not only increase the amount of catalyst volume but also the heat transfer area for the same membrane surface area. It was found that at the same molar feed rate of ethylbenzene, the larger the reactor diameter, the higher

the conversion; however, the improvement was less significant at large diameter. The temperature profile shown in Figure 5.15 revealed that the temperature in the bed dropped with the increasing diameter. The larger diameter value, the higher temperature drop at the beginning of the bed because of higher extent of reaction, which resulted in the higher heat consumption. The temperature started increasing again because the rate of heat transfer to the catalyst bed is higher than the rate of heat of reaction. The larger reactor diameter showed higher rate of temperature increase because of high heat transfer area. From the previous studies it was expected that increasing W_{cat}/F_{EB0} (by increasing the reactor diameter) did not only increased the conversion but also decreased the selectivity. However, for this study, the rather constant selectivity at 87% was observed. These results can be explained by considering the effects of W_{cat}/F_{EB0} and temperature on the performance of the reactor. Increasing W_{cat}/F_{EB0} trended to give higher conversion but lower selectivity. On the other hand, decreasing temperature trended to give lower conversion but higher selectivity. These two competing effects obviously affected the performance of the reactor. In addition, the effect of radial dispersion should be taken into account. Figure 5.16 shows the profiles of the differences of temperature and partial pressure of hydrogen between the reactor wall and the membrane surface. It was found that the effect of radial dispersion become more pronounced with the increasing reactor diameter. The presence of the radial dispersion retarded the rate of hydrogen removal from the reaction zone and, consequently, the shift of the forward reaction. It can be concluded from this study that increasing the reactor diameter which affected the amount of catalyst and the heat transfer area of the reactor increased the yield of the reactor; however, after approaching an optimum value the increase of the reactor diameter did not improve the reactor performance. Hence, selection of an optimum reactor diameter was an important design parameter for the success of the membrane reactor operation.